about the same for single-beam and for spherical irradiation. This contrasts with our finding for 1.05-μm irradiation that $\dot{m}$ for spherical irradiation is about *three times higher* than most reported results for the single-beam case.

These observations provide an improved understanding of transport. Nonlocal heating results in a more gradual temperature drop into the target which is consistent with the results of Fig. 11. This "smearing" of the heat front results from the longer mean free path of electrons in the tail of the thermal-electron velocity distribution. We expect these effects to diminish in importance as we move to shorter-wavelength irradiation because of the increased critical density (and, in addition, a lower temperature if different wavelengths are compared at the same absorbed irradiance).

In order to understand better the impact of the multi-energy-group nature of transport one needs to incorporate the equivalent of a Fokker-Planck treatment[5] into a hydrodynamic code. This has been done using an approximation (a "hybrid" treatment) which greatly economizes computation time while preserving the essential multi-group, nonlocal character of transport. Another important consideration is that the excitation rates of the x-ray lines used are changed in the presence of non-Maxwellian electron distributions. Theoretical analysis of these experiments taking these developments into account is now in progress.

REFERENCES

1. B. Yaakobi, T. Boehly, P. Bourke, Y. Conturie, R. S. Craxton, J. Delettrez, J. M. Forsyth, R. D. Frankel, L. M. Goldman, R. L. McCrory, M. C. Richardson, W. Seka, D. Shvarts, and J. M. Soures, *Opt. Commun.* **39**, 175 (1981).
2. T. J. Goldsack, J. D. Kilkenny, B. J. MacGowan, P. F. Cunningham, C. L. S. Lewis, M. H. Key, and P. T. Rumsby, *Phys. Fluids* **25**, 1634 (1982).
3. B. Yaakobi, J. Delettrez, L. M. Goldman, R. L. McCrory, W. Seka, and J. M. Soures, *Opt. Commun.* **41**, 355 (1982).
4. Rutherford Laboratory Annual Report RL-81-040, Chap. 4.4 (1981).
5. A. R. Bell, R. G. Evans, and D. J. Nicholas, *Phys. Rev. Lett.* **46**, 243 (1981).

2.C High-Resolution Harmonic Photography on OMEGA

The study of harmonic emission from spherical targets irradiated by intense laser light is of interest for several reasons. Two-dimensional harmonic photography, particularly of the $2\omega_0$ and $3\omega_0/2$ emissions, has long been used as a signature of the critical (n_c) and quarter-critical ($n_c/4$) surfaces. The $2\omega_0$ emission is generally believed to originate from the critical density surface, as a second-order overtone

of the driving electric field during resonance absorption, and the $3\omega_0/2$ emission from the quarter-critical density surface due to the interaction between incident radiation at frequency ω_0 and plasma waves at $\omega_0/2$ generated by plasma instabilities such as the two-plasmon ($2\omega_{pe}$) instability.[1] Thus, two-dimensional photography of these harmonics permits the measurement of the excursions of both the critical and quarter-critical density surfaces during the irradiation of the target.[2]

Since both critical-density and quarter-critical-density phenomena are intensity sensitive, high-spatial-resolution harmonic photography may be used to give an indication of the overall uniformity of irradiation of targets under multi-beam illumination. In addition, analysis of the spectral and temporal characteristics of harmonic emission, particularly the $3\omega_0/2$ emission, shows considerable potential as a means of diagnosing the coronal electron temperature; this analysis also aids in the understanding of those processes which produce hot electrons deleterious to efficient target implosions.

Studies of the harmonic emission from spherical targets irradiated by the 1.053-μm, 24-beam OMEGA laser facility were performed with the instrumentation shown in Fig. 13. A high-resolution (2-μm) binocular camera system was used to obtain photographs of the second-harmonic and 3/2-harmonic emissions in a common viewing direction.

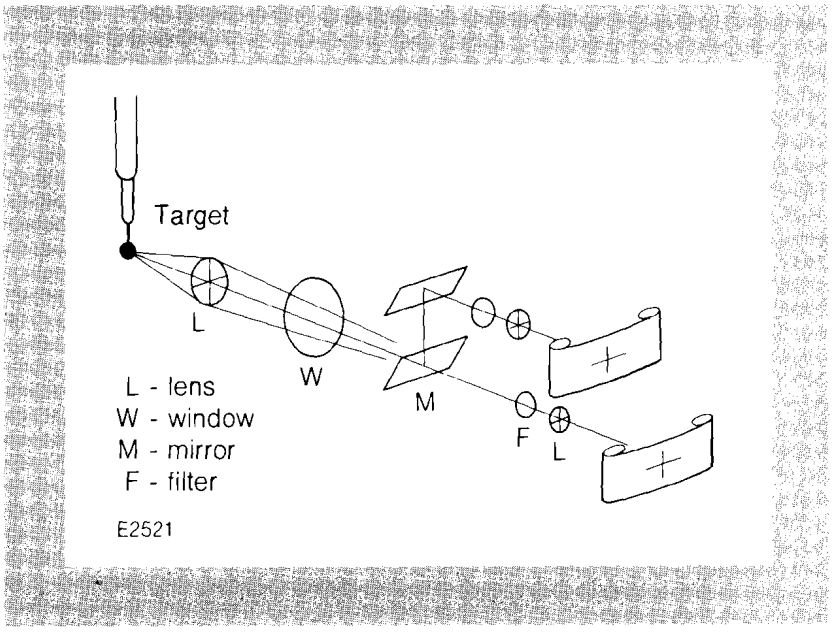

Fig. 13
Experimental setup on OMEGA used for the analysis of harmonic emission from spherically irradiated targets. This setup enables the target to be simultaneously photographed in two different wavelengths from the same direction.

Typical photographs of the second-harmonic and the 3/2-harmonic emissions originating from a uniformly irradiated glass microballoon are shown in Fig. 14. This large-aspect-ratio target ($R/\Delta R \sim 200$), of 400-μm diameter and DT-filled, was irradiated uniformly with a 1-ns pulse at an average intensity of 3.6×10^{14} W/cm^2. The three photographs show the original target size and the $2\omega_0$ and $3\omega_0/2$ emissions on a common spatial scale.

Several features in these harmonic-emission photographs are apparent. The principal component of the second harmonic originates

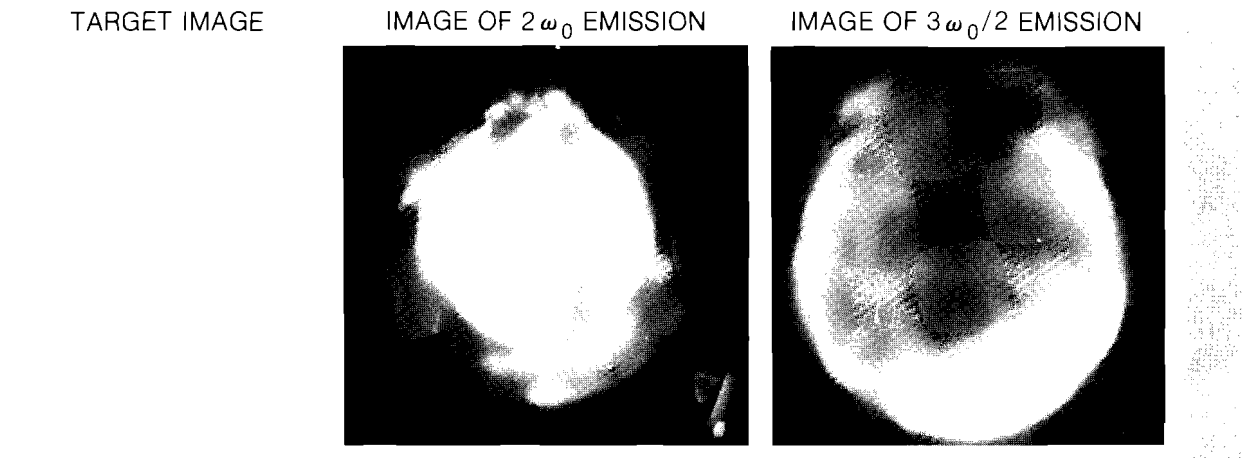

Fig. 14
Spatially resolved $2\omega_0$- and $3\omega_0/2$-harmonic emission from a 420-μm-diameter, 1-μm-wall-thickness, DT-filled glass microballoon irradiated uniformly with 24 beams at an intensity of 3.6×10^{14} W/cm^2 for 1 ns. The outer component of the second-harmonic emission is believed to originate from the quarter-critical region.

from a region similar in diameter to that of the original target. The $3\omega_0/2$ emission, on the other hand, originates from a region considerably greater in extent and exhibits a fairly sharp outer boundary. In both harmonics, the perturbing effect of the stalk support on the symmetry of the underdense corona is clearly visible.

The spatial scales of the second-harmonic and 3/2-harmonic emissions are in broad agreement with what is expected on the basis of one-dimensional *LILAC* code calculations. This is illustrated in Fig. 15,

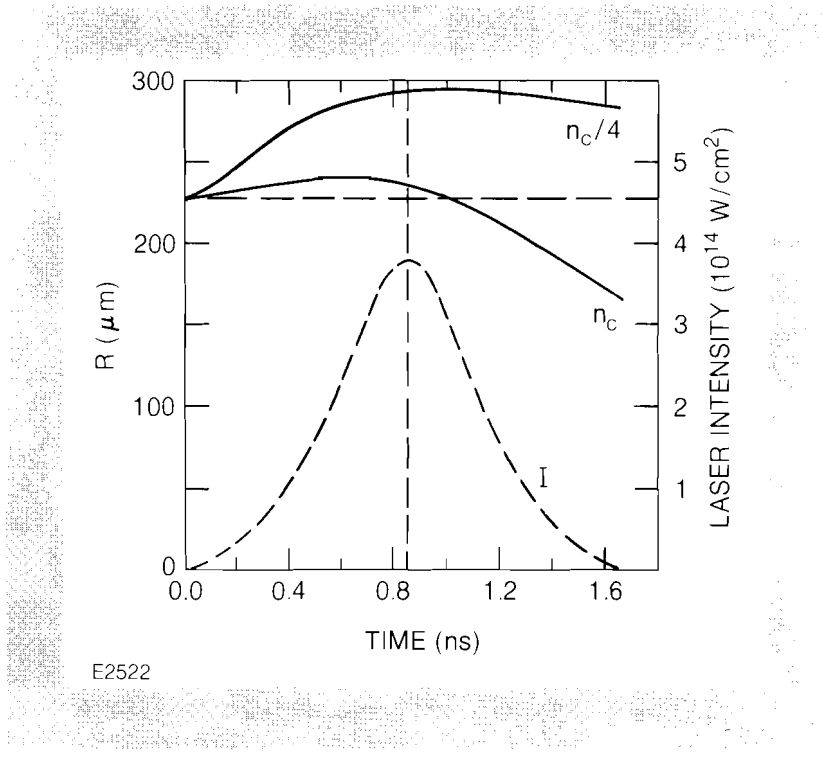

Fig. 15
One-dimensional code predictions of the trajectories of the n_c and $n_c/4$ surfaces for a 450-μm-diameter, 1-μm-wall-thickness, DT-filled glass microballoon irradiated at 4×10^{14} W/cm^2. The dashed curve indicates the time history of the incident laser intensity (relative to the initial target radius).

which shows a simulation of the trajectories of the critical and quarter-critical densities throughout the duration of the laser pulse. The irradiation conditions are similar to those that were used in obtaining the data in Fig. 14. The simulation assumes absorption on a self-consistent density profile, principally by inverse bremsstrahlung, with a 10% deposition of the radiation reaching the critical surface into fast electrons having a temperature prescribed by the Livermore model of resonance absorption.[3] In addition, the simulation utilizes a flux-limited prescription for thermal transport with a value of $f = 0.05$. As can be seen, the simulation predicts little excursion of the critical surface during the laser pulse while showing an excursion of approximately 100 μm for the quarter-critical region. This is in close agreement with the spatial scales of the harmonic emission.

Figure 14 shows that, in addition to the predominant second-harmonic emission from a region of the target equivalent in size to the original target diameter, there is evidence for a secondary component having a spatial scale and general morphology similar to that of the 3/2-harmonic emission. This would suggest the generation of $2\omega_0$ emission from the $n_c/4$ region, an observation that has not previously been made. Some additional experiments have been performed to characterize further this secondary component of the second-harmonic emission. Figure 16 shows harmonic photographs of a small target irradiated with 1.3-ns pulses at an intensity of 1.5×10^{15} W/cm^2. Under these conditions the penumbral second-harmonic emission is of greater intensity than the emission originating from the critical-density region and still displays spatial characteristics similar to the $3\omega_0/2$ emission.

Fig. 16
Variation of spatial characteristics of harmonic emission with irradiation intensity. This 192-μm-diameter glass-microballoon target was uniformly irradiated with an intensity of 1.5×10^{15} W/cm^2. These harmonic images should be compared with those of Fig. 14.

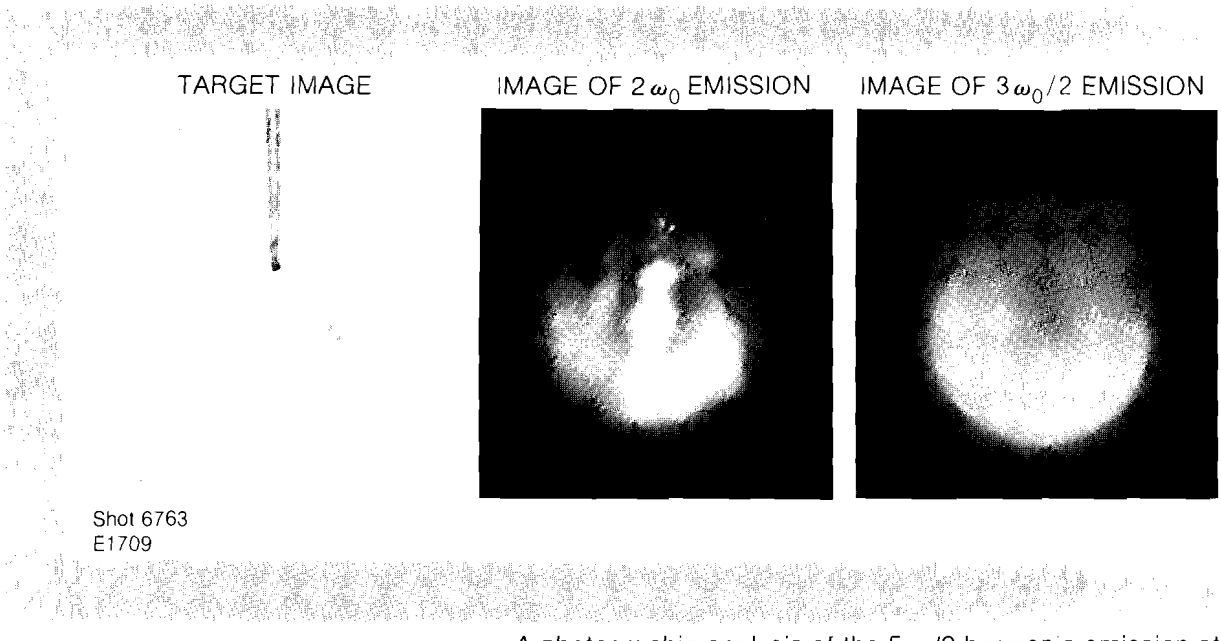

A photographic analysis of the $5\omega_0/2$-harmonic emission at 4230 Å has also been made. Figure 17 shows a typical image of the $5\omega_0/2$ emission from a ~400-μm-diameter, 1-μm-thick DT-filled glass microballoon, irradiated uniformly at 4×10^{14} W/cm^2. This emission also appears to originate from the quarter-critical region.

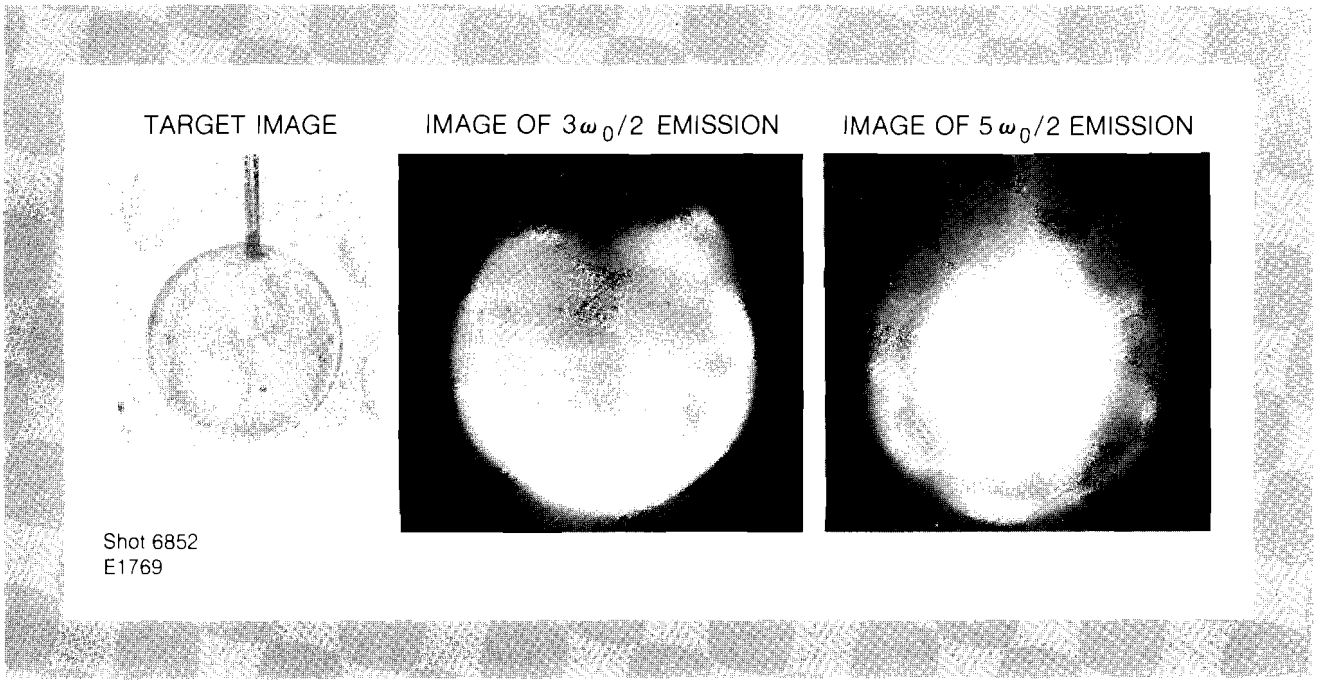

Fig. 17
Comparison of the spatial distribution of the $3\omega_o/2$- and $5\omega_o/2$-harmonic emissions from a uniformly irradiated 415-μm-diameter, 1-μm wall thickness, DT-filled glass microballoon irradiated at $4x10^{14}$ W/cm^2. The $5\omega_o/2$ emission also appears to originate from the quarter-critical region.

Photography of the extent of the harmonic emission can also be used to identify nonuniform and microstructural effects in the underdense corona. This is illustrated in Fig. 18 which shows the harmonic emission from a 235-μm-diameter glass microballoon overcoated with Cu (2 μm), Al (2 μm), and CH (10 μm). Targets of this type were recently used in analyzing thermal transport in spherical geometry (see Section 2.B in this issue). In general, targets having a low-Z outer layer displayed interesting features in the underdense corona. In particular, the 3/2-harmonic emission showed strong evidence for small-scale microstructures at the quarter-critical surface, as can be seen from Fig. 18. Although this structure is clearly visible at the quarter-critical surface, the second-harmonic photograph taken from the same direction shows little evidence for similar structure at the critical-density surface.

Summary

Photographic analysis of the harmonic emission from spherical targets irradiated with the multi-beam OMEGA system has led to many interesting findings. The excursions of the critical and quarter-critical surfaces, as determined from $2\omega_o$ and $3\omega_o/2$ emissions respectively, are in broad agreement with one-dimensional code calculations assuming inverse-bremsstrahlung absorption and a flux-limited thermal transport model (with $f = 0.05$).

The study of the spatial distribution of the harmonic emission has been a valuable addition to the ongoing studies aimed at estimating the level of irradiation uniformity achieved on OMEGA.[4] Finally, the spectral and temporal characteristics of the harmonic emission have the potential for increasing our understanding of instability phenomena occurring in the underdense region. These features of the harmonic emission have been studied in greater detail and will be described in a forthcoming issue of the LLE Review.